Solid Freeform Fabrication 2022: Proceedings of the 33rd Annual International Solid Freeform Fabrication Symposium – An Additive Manufacturing Conference
Reviewed Paper

IN-SITU MONITORING OF LASER-POWDER-BED-FUSION USING IR AND NIR EMISSIONS TO DETECT THERMAL ANOMALIES

M. A. Roach*, B. Fowler*, D. Thakkar**, C. Babbitt**, S. Khurana**, B. H. Jared*

*Mechanical, Aerospace and Biomedical Engineering, University of Tennessee, Knoxville, TN 37919
**Addiguru, USA

Abstract

Process monitoring of laser-powder-bed-fusion (L-PBF) has advanced significantly since the beginning of this technology. Many methods exist today for in-situ process monitoring; however, these methods can be costly to implement and provide sub-par image resolutions. This research aims to develop a method of low-cost and high-resolution thermal monitoring system using near-infrared (NIR) wavelength band emission monitoring to detect anomalies. This research will compare more expensive infrared (IR) wavelength band monitoring methods to the cheaper NIR method and other drawbacks brought about by monitoring one wavelength band over the other.

Introduction

There exist many methods of monitoring L-PBF that can be implemented for several types of equipment in a vast variety of printable materials. One such monitoring method is the collection of specific wavelength emissions during and after the melting and solidification process for L-PBF with atomized metal powder. This can provide information about the health of the equipment, but more importantly, this can provide information that correlates with the quality and properties of the printed material.

For this experiment, a hypothesis was formed that by using NIR process monitoring of the build surface during and after the printing of materials, information about the quality and properties of the final material can be correlated with the collected NIR sensor information. To assess this hypothesis, a thermal testbed was initially set up to prove the ability to collect thermally correlated data using a NIR camera. The equipment from this testbed setup was then moved into the L-PBF system for testing in simulated and actual printing environments.

This hypothesis was based upon the knowledge of NIR signal emissions of black bodies at known temperatures, as well as a NASA patent that was exploring the ability to correlate NIR and IR signals from L-PBF processes to re-construct a 3D representation of the build detect thermal anomalies, in the form of visually identifiable “hot-spots” [1]. The setup for the NASA research can be seen in Figure 1. Initially, the experiment outlined in this paper was aimed toward replicating this setup, however, it was seen that using only the NIR camera was still able to yield meaningful results without the need for an infrared camera.

The use of IR cameras in L-PBF is also not uncommon and has been proven as a viable method of process monitoring [2]; however, common IR cameras are very expensive, hard to connect, and tend to have low-resolution sensors and slow frame rate for image capturing. These challenges have all been seen through past research experiences using IR cameras. By using a NIR camera as the main process monitoring sensor, it should allow for a less-expensive, higher-resolution, and easier image capture capabilities. This should allow for more granular process monitoring during the build cycle, including the ability to adjust collection parameters to detect different forms of anomalies, which is not possible using traditional IR cameras.

A common IR camera used in our research is the FLIR® A35 which yields a resolution of 320 by 256 pixels, 60 frames-per-second, and a resale cost of approximately $6000 at the time of writing this manuscript. The NIR camera used for this experiment was the Pixelink® PL-D734MU-NIR-T which yields a resolution of 2048 by 2048 pixels, 90 frames-per-second, and a cost of $2200. By using the NIR camera for process monitoring, the smaller nominal pixel size of the sensor allows for geometrical accuracies which are far more

meaningful than those possible with standard IR cameras. The drawback of using a NIR camera over an IR camera is the loss of temperature accuracy. This research also aims to prove that, in L-PBF monitoring, an accurate temperature is not as valuable as the detection of temperature variations for correlation with certain process defects, such as bulk porosity; therefore, using a NIR camera is a useful method of process monitoring. [3], [4]

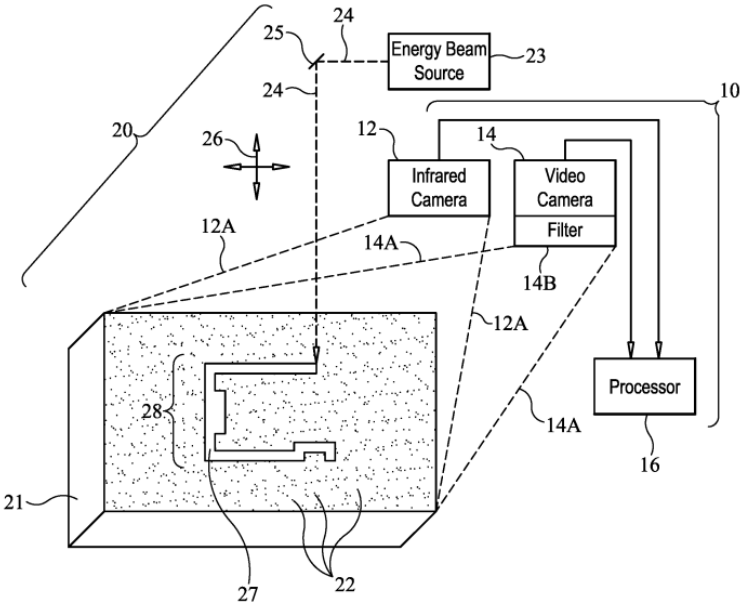

Figure 1: Setup image from US Patent 10,688,560 L-PBF IR and NIR process monitoring setup. [1]

Experimental Setup

There existed two main experimental setups for this research. The first consisted of the monitoring equipment and a simulated heat source in a controlled lab environment. This was done initially to decide upon the validity of using a NIR camera as a method of thermal process monitoring. Once this capability of the NIR camera was confirmed and configured, the same equipment was then installed into the L-PBF system for both simulated and actual printing processes to explore its use as a process monitoring system in the additive manufacturing environment.

Testbed Experimentation

The first testbed setup consisted of the Pixelink NIR camera with a band-pass filter of 700 nm, a FLIR IR camera, a standard ceramic hotplate capable of reaching 500°C, and various test artifacts of dissimilar materials and surface finishes. This setup can be seen in Figure 2. This testbed setup allowed for the selection of a proper camera configuration with exposure time and camera aperture. The band-pass filter was selected to filter all non-useful wavelengths from the laboratory background while still allowing for the collection of useful wavelengths generated by the heat source and test artifacts.

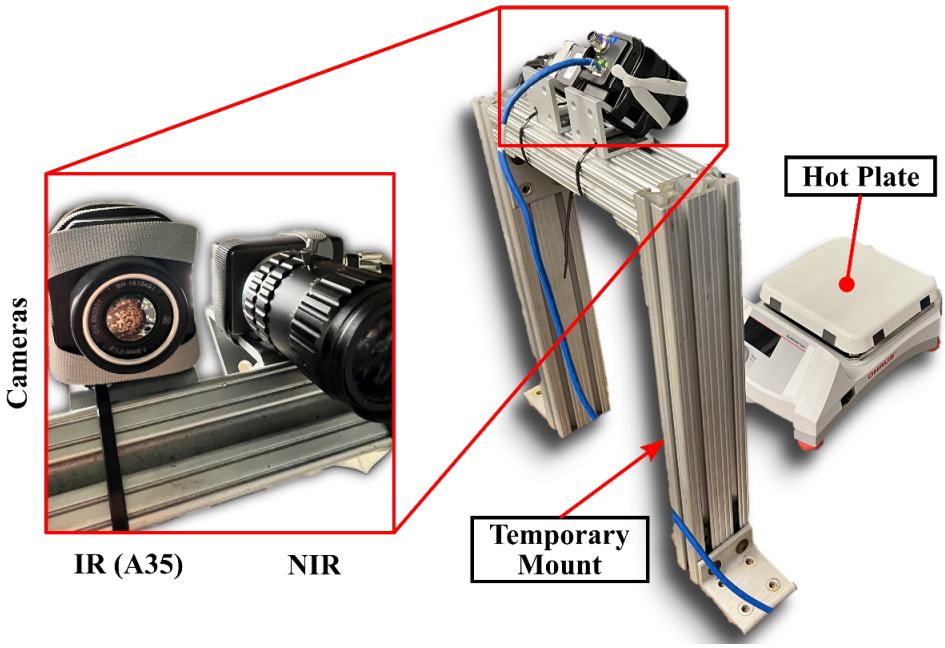

Figure 2: Thermal testbed setup for initial NIR and IR camera exploration.

The initial testbed setup performed to explore the use of the NIR camera consisted of two main experiments. The first was the use of a test piece of aluminum with a reflective surface. The second was the use of multiple dissimilar materials of varying emissivity. For the first experiment, the aluminum piece was placed on the hotplate and heated from room temperature to 500°C. The NIR and IR cameras were set to record over the duration of the heating. Upon reaching the set temperature, the IR camera showed an increase in detector intensity on the hotplate and a less-significant increase of intensity seen on the aluminum sample as seen in Figure 3. This can be explained by the differences in emissivity of the hotplate and the aluminum piece.

During the second experiment, four different test pieces were run through an identical experiment as in the first experiment. The four pieces consisted of pieces made of matte aluminum, brass, black-oxide alloy steel, and reflective aluminum. Once at the set temperature, the brass, steel, and matte-finished aluminum, as well as the hotplate surface all, showed an increase in detector intensity on the IR camera, while the reflective aluminum showed little intensity change like in the first experiment. Looking at the NIR camera signals, it can be seen there was an increase in detector intensity around the reflective aluminum piece as well as the hotplate surface surrounding it. These results can all be seen in Figure 3.

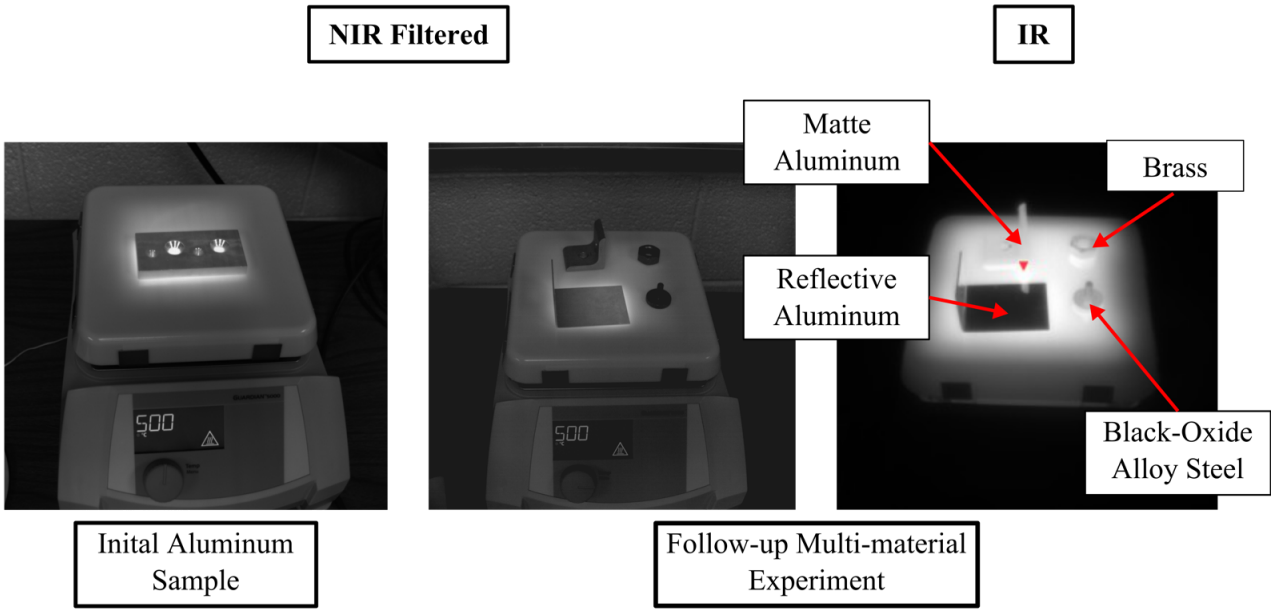

Figure 3: Thermal testbed preliminary results.

After the preliminary results of the testbed experiments showed a qualitative correlation between NIR detector intensity and thermal conditions, a third experiment was designed to quantitatively analyze these observations. This last experiment consisted of the same hotplate and the aluminum piece from experiment one and followed the same heating set point. The aluminum piece was not of a known temperature as a thermocouple was not installed on this system. The hotplate temperature is known by using the internal thermocouple of the hotplate, used for heating control, and can be compared to the recorded detector values of both the NIR and the IR cameras. This was done by comparing the hotplate temperature to a set point on the plate surface, as seen in Figure 4. The detector values from this point on both cameras were recorded over the length of the heating cycle. The results can be seen in Figures 5 and 6.

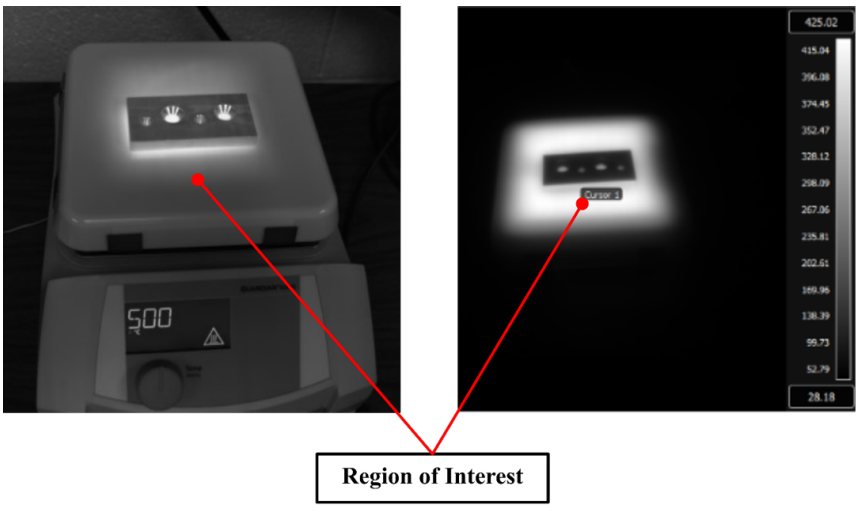

Figure 4: Hotplate set point location for both IR and NIR cameras.

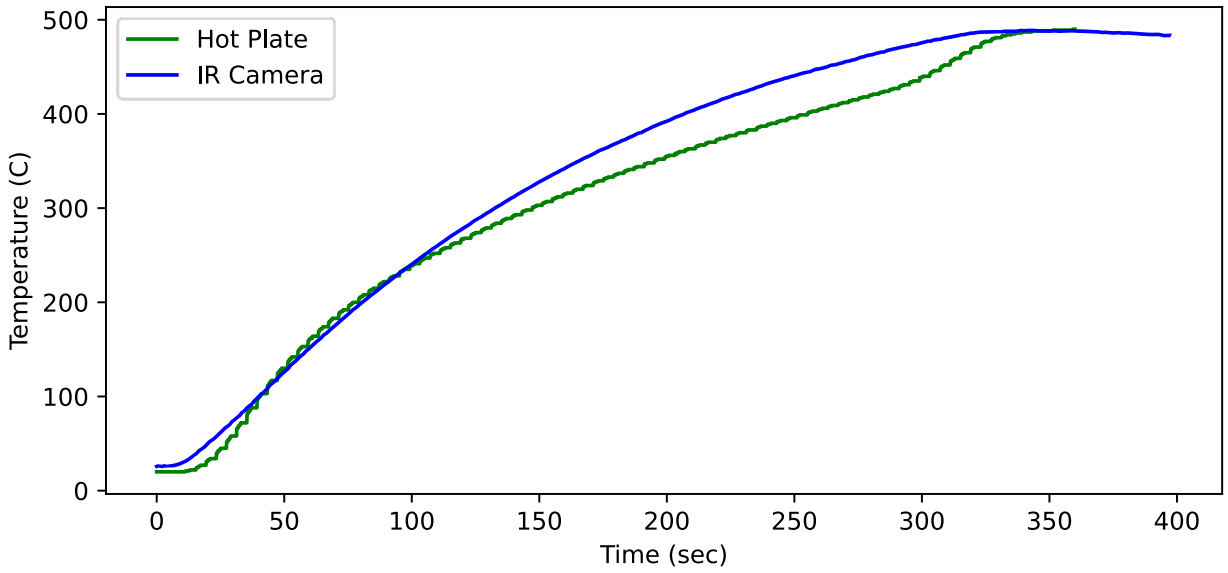

Figure 5: Comparison of the hotplate temperature to IR detector results.

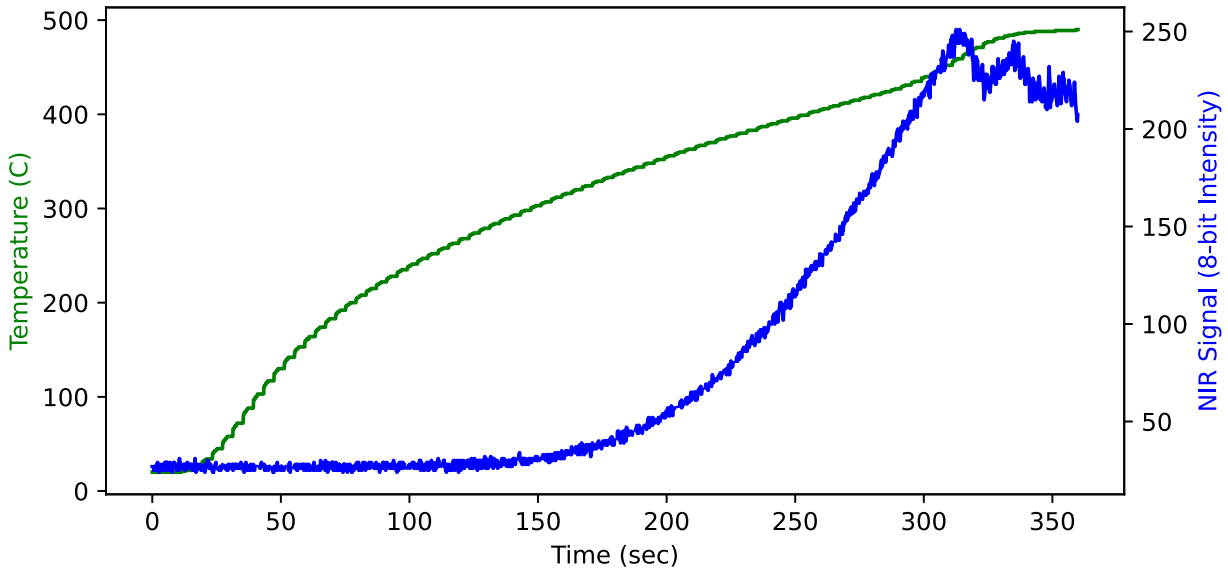

Figure 6: Comparison of the hotplate temperature to NIR detector results.

The IR signal data corelates well to the hotplate temperature, while the NIR signal begins to exponentially increase in intensity after about 100 seconds, or around 200-300°C. Towards the end of the heating cycle, the NIR signals appear to oscillate near the 500°C setpoint. When comparing back to the NIR recorded frames, the plate stays close to the setpoint temperature, however the heating element is occasionally seen emitting brighter and dimmer, most likely due to the heating control unit of the hotplate regulating the setpoint temperature. Through this experiment it can be seen that a NIR camera can detect thermal changes and can be further explored within the L-PBF system.

System Installation and Configuration

Both the NIR and IR cameras were installed in the Farsoon FS271M L-PBF system where the NIR camera was mounted outside the system with a view through a fused silica window capable of transmission wavelengths in the range from 200 to 2200 nm. The IR camera was installed inside the system with no other filtering. Both cameras were viewing the build plate at an angle of between 15-30 degrees, and at a distance like the testbed setup which was around 50cm. The setup can be seen in Figure 7.

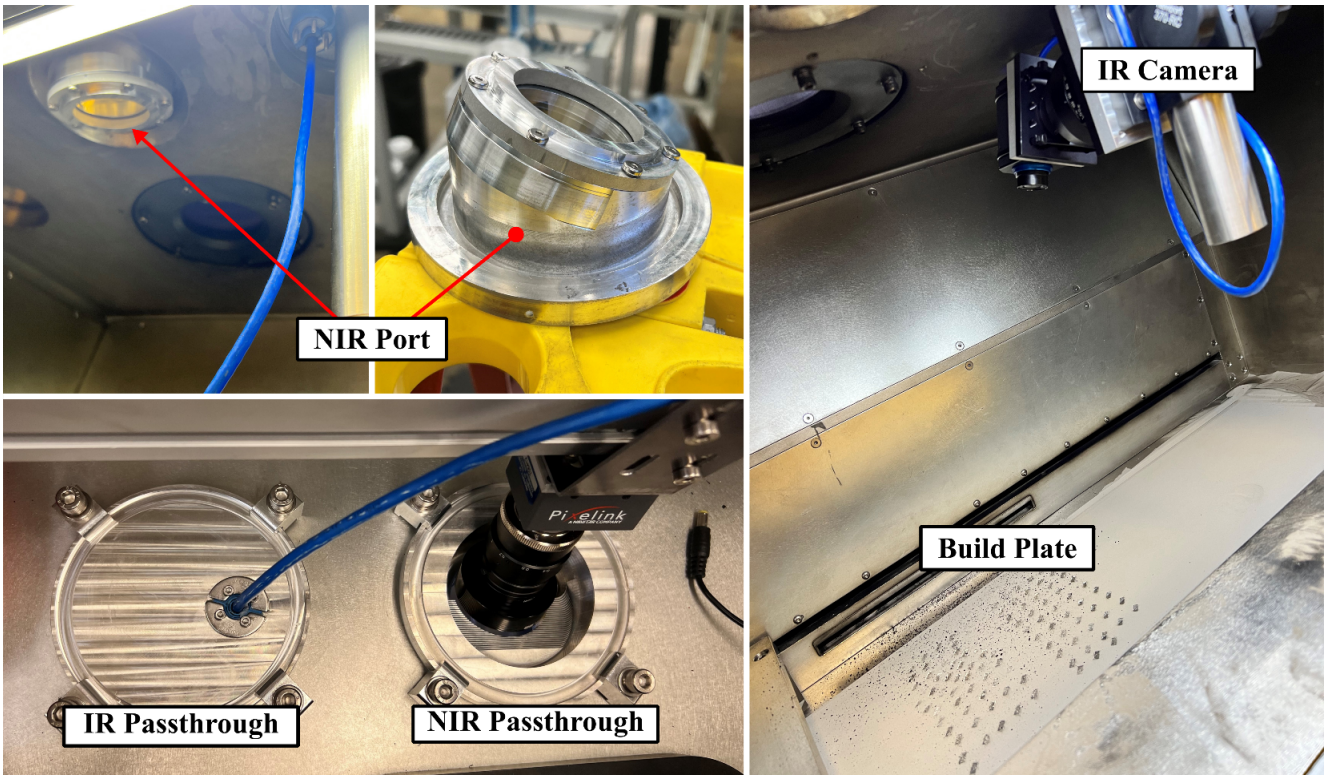

Figure 7: System installation photos.

Due to the high-intensity emissions generated by the laser, a new filter is needed to remove excess emissions to yield a more meaningful image of the printing process. To yield the most meaningful data, without saturating the NIR sensor, an optimal combination of exposure time and filter configuration was needed. To find the most optimal range, 30 different filter and exposure time configurations were tested, all of which are outlined in Figure 8.

In each of the experiments detailed below, the laser was fired on a bare build plate with nominal build parameters. There was a series of 8 squares positioned on the build plate to allow for image correction and to identify any possible locations for laser reflection. The filter configuration of the camera as well as the exposure time was changed for each of the experiments as a single layer was deposited without powder on the stationary build plate. The NIR camera was set to record the entire duration of laser-firing. These data were exported from the system as a series of image frames.

Using Python and OpenCV, the sequence of images was analyzed and the intensity of each pixel location in the subsequent image was summed into a matrix. This matrix is the total intensity experienced

by a select NIR pixel throughout the entire laser-firing. These results are shown as the color images in Figure 8.

	30µs	60µs	100µs	500µs	1ms	5ms	10ms
No Filter	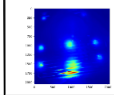		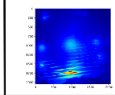		Not Collected	Not Collected	Not Collected
700nm Bandpass	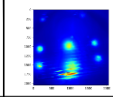		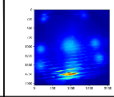				Not Collected
813 - 948nm	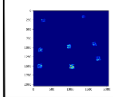		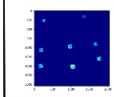				Not Collected
747 - 757nm	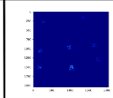		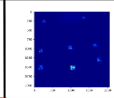				
900 - 950nm	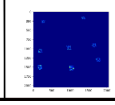		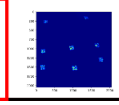				

Figure 8: System simulated experiment; varying exposure times and NIR camera filters.

An exposure time between 30 and 100 microseconds with a filter of ranges 813 – 948nm, 747 – 757nm, or 900 – 950nm (bottom 3 filters and leftmost 3 exposure times) yield an image without excess reflections and ghosting, as seen in Figure 9 on the left- and right-most images. These reflections can be seen much more dramatically in higher exposure times and less restrictive filters, which overwhelms the laser intensity data intended to be captured. The configuration selected from this set of experiments to continue with for further experimentation was an exposure time of 60 microseconds and a filter of range 900 to 950 nanometers. This configuration was selected as it yielded a high-rate capable exposure time and did not over-saturate the sensor with ghosting or reflections.

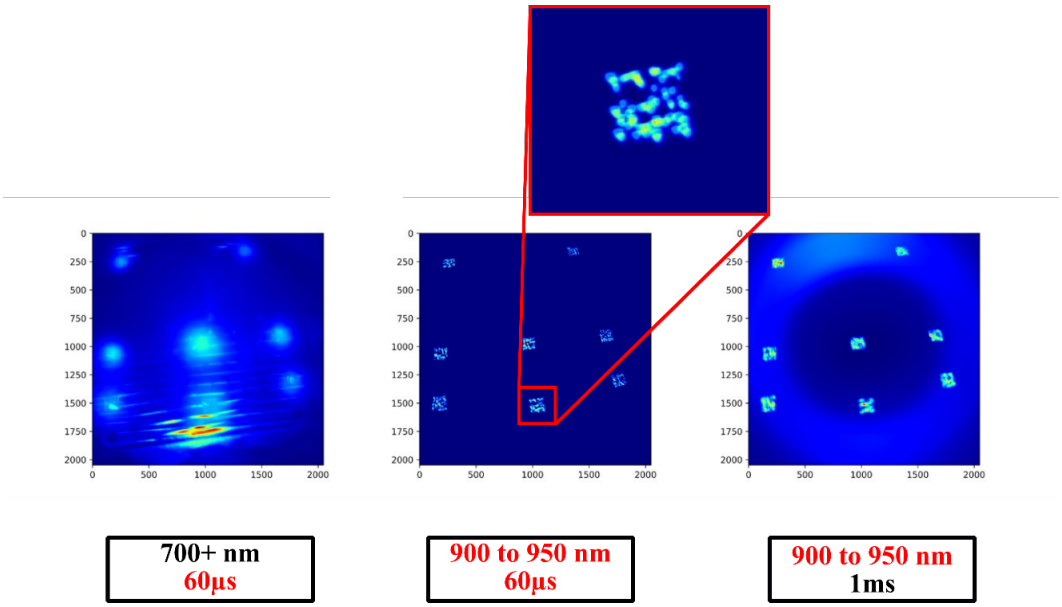

Figure 9: Over-exposed (left and right) and ideal (center) filter and exposure time configurations.

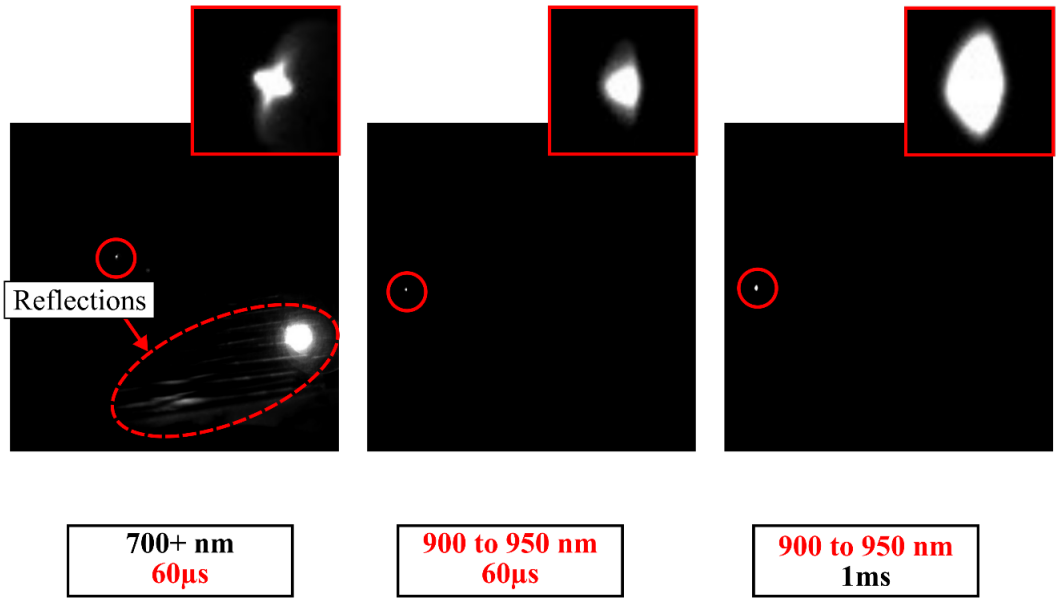

Figure 10: Single frame NIR captured data from selected configuration (center) and over-exposed configurations (left and right).

Another aspect of this research was to figure out if the NIR camera can detect inter-layer temperature, or the temperature of the powder bed after the completion of a single layer. In order to detect inter-layer temperature, the NIR sensor must be capable of exposing for extended amounts of time. It was seen that an exposure time beyond 5 seconds with no background NIR interference, taken within 2 seconds of the laser firing on the build plate showed no detectable increase in intensity. Due to the time between laser-firing between layers being 13 seconds, with the powder wiper bar of the Farsoon obstructing the build plate view for most of this time, it was decided that using the NIR camera for post-solidification thermal monitoring was not plausible using the current setup. Future experiments focused on the analysis of the laser spot size data from the frames of the NIR data, as seen in Figure 10.

Induced Failure Experiment Design

A test build was developed to induce defects in printed parts by varying the fill laser power part parameter while using all other nominal settings as defined in Table 1. These powers ranged from 100 to 400 watts in increments of around 75 watts. Parts at 100 watts are designed to yield lack-of-fusion defects while the 400-watt parts are designed to melt and solidify near the peak energy capability of the system.

Table 1: Process parameters used for all samples.

Parameter	Value
Scan velocity	1000 mm/s
Layer thickness	30 µm
Base plate temperature	100 °C
Hatch spacing	120 µm

There are seven unique geometries printed in this build. There were three sizes of 10mm tall cylinders including 5-, 10-, and 15-mm diameter variations as seen in Figure 11, images A, B, and C. There were three parts printed to induce part over-heating as seen in images D, E, and D. Finally, there was a 10mm cube. These geometries were placed evenly spaced on the build plate in as seen in Figure 11, and their respective build parameters in Table 2.

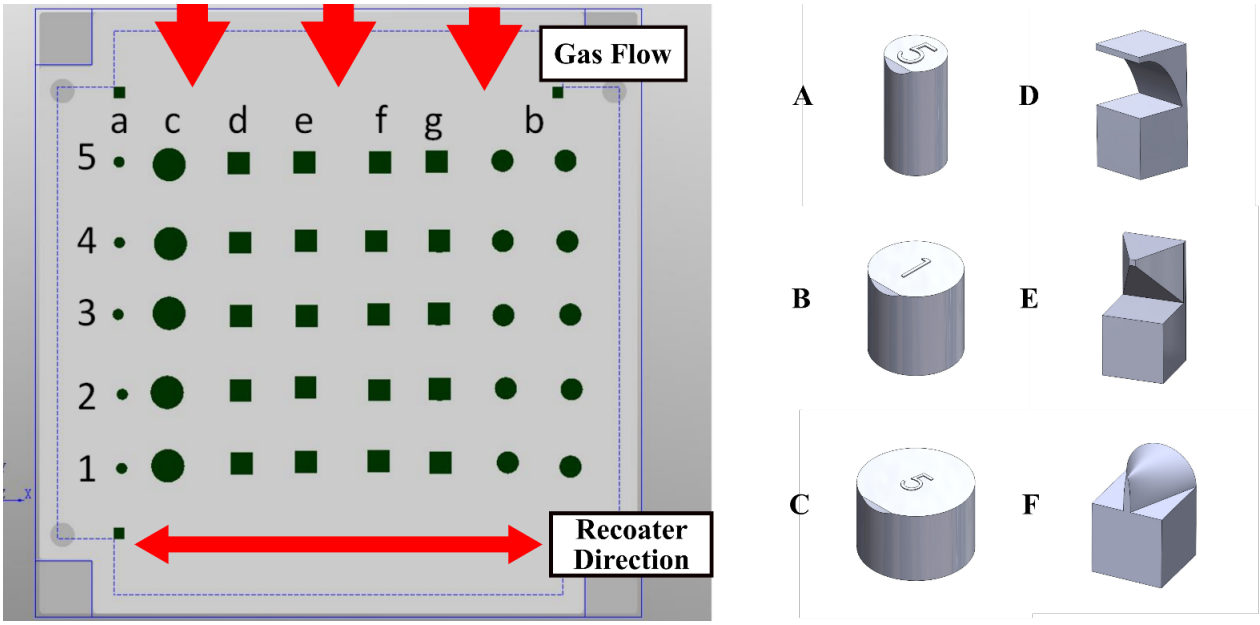

Figure 11: System experimental setup.

Table 2: Modified fill laser power

Row Number	Modified Fill Laser Power (W)
1	100
2	175
3	225
4	325
5	400

Experimental Results

The induced defect experiment designed above was ran in the Farsoon L-PBF system with the same NIR and IR camera setup decided upon after the lens filter and exposure time selection experiment. The system used nitrogen as the inert gas and powder atomized 316L stainless steel powder as the metal. After the experiment was run, the IR and NIR data were processed and analyzed. These results can be seen in Figure 12, with more detailed processes found in the following sections. For scale, the parts in columns labeled d, e, f, g, and b (from Figure 11) are all 10 mm in size and all parts are 10 mm tall.

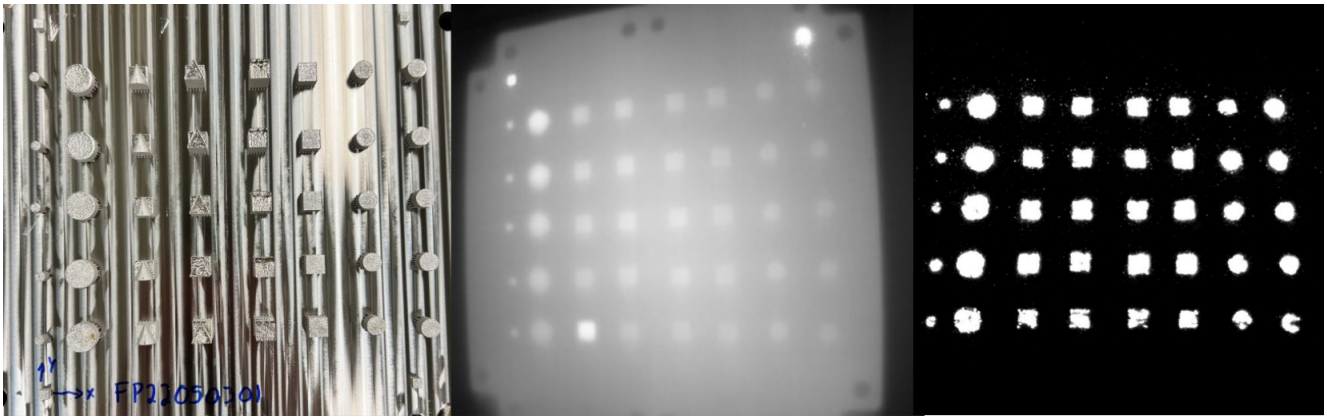

Figure 12: System actual printing experiment; raw results for IR and NIR cameras.

IR Reference Data

The FLIR A35 was used to collect infrared thermal data to allow for correlation with the NIR collected data for locations of high and low thermal radiation or to further investigate specific changes noted in the NIR data. In Figure 12 you can see a frame captured from an arbitrary layer by the IR camera. As parts are solidified, they appear brighter in intensity and cool over time to a lower intensity. One of the parts on the lower left appears to be higher in intensity than all others near it, this is because it was fired upon more recently in reference to when this frame was captured. IR data is still useful in the process monitoring of L-PBF, and in combination with the NIR data collected from this experiment, more insights into the process may be discovered. This exploration will take place in future research as the NIR and IR data will be combined, and thermal gradients extracted.

NIR Data

The NIR camera was set to collect data throughout the entire build with the configuration outlined in the experimental setup. This data was collected as a series of images for each frame recorded by the camera. This image stack was then processed using Python and OpenCV to isolate the specific attributes. It was first filtered to remove pixel values of 5 or lower. It was seen that including these pixel values in a layer-wise sum of the frames contribute to the noise of the camera sensor. These pixel values were removed by overwriting them with a value of 0.

The image processing algorithm was used to calculate the total pixel intensity over each layer. For example, if a single pixel was full brightness (255) for two frames in the video, and off (0) for the rest of the video, the final pixel intensity would equal 510. The resulting data can be seen in Figure 12 as the greyscale image on the right. Parts shown on the top in all images of Figure 12 are printed at the highest laser power while parts on the bottom are printed with the lowest. The parts in between are scaled as seen from Table 2. As laser power increases, the shape of the part becomes clearer, and the amount of spatter also increases. The lower-power parts are more globular in shape and lack spatter; higher-power parts are more defined and present significantly more spatter.

To detect changes in thermal signatures better, the image from the NIR cumulative data in Figure 12 was converted to a color map with more dramatic changes visible in higher-value pixels. These results can be seen in Figure 13 where a laser power increase is now shown from left to right.

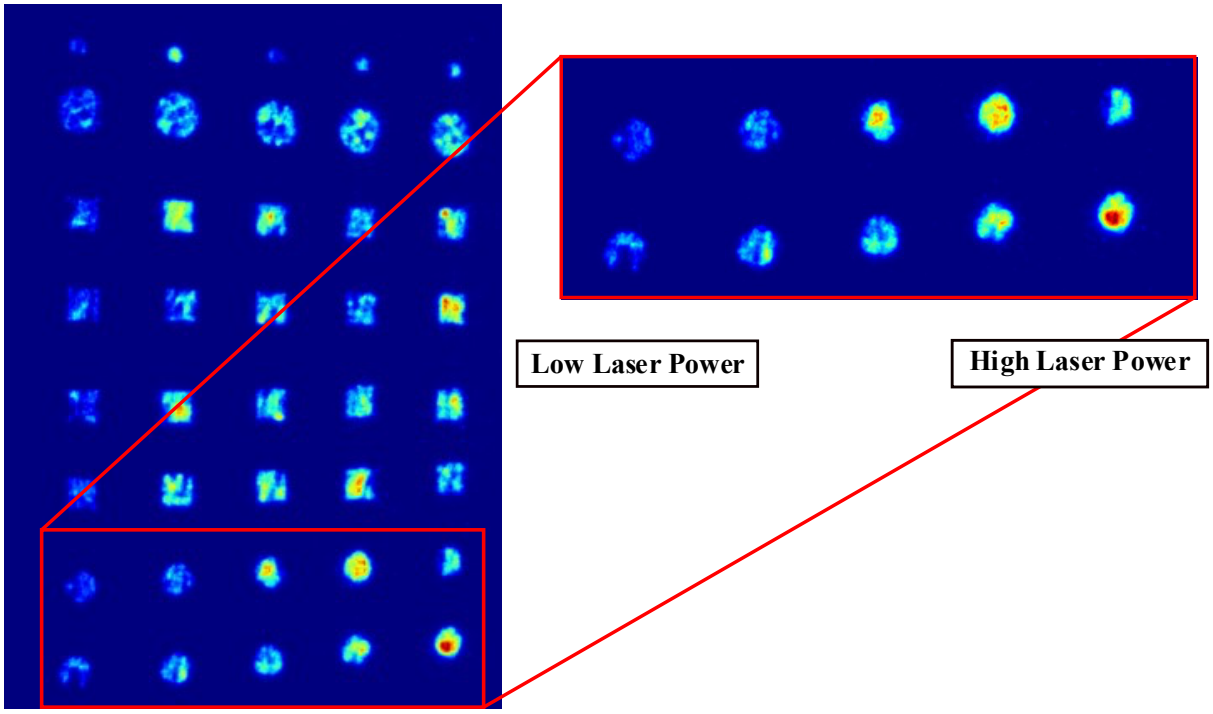

Figure 13: Analyzed NIR signal information.

The 10 mm diameter cylinders were the focus for the rest of the experiment, as they were the simplest geometry that could be reasonably scanned in post-processing equipment. Future research will be conducted to evaluate the other geometries, specifically the defect inducing geometry.

The colormap image and zoomed-in detailed portion seen in Figure 13 clearly show that, in general, the NIR signal data increases in intensity as laser power increases. This can be seen as a change in the colormap scale (Python Jet) where blue is the lowest, and red is the highest intensity. By combining this layer-wise NIR data in series with all other printed layers, it becomes possible to re-create a model of the NIR signals in a spatial reference frame and allow for the ability to identify areas of concern. While this research timeline was short, the re-creation of each layer's NIR was not able to be processed, the single layer was used in correlation with other post-processing data collection to find correlations between NIR layer-wise data and part density.

CT Analysis

Upon completion of the build, there were 10 samples of the 10 mm cylinders which were further analyzed using x-ray CT. There were two samples for each laser parameter configuration. The results can be seen in Figure 14 in the last row of images for the first 5 of these cylinder samples. These images were generated from an arbitrary layer within the given part. The CT data was collected by a 225 KeV x-ray CT system with a 9.48 μm voxel size. The data was post-processed with ring removal, beam hardening correction, intensity equalization in Z-slices, background removal, and followed by thresholding segmentation to segment pores.

Data Correlations

To correlate the NIR signal intensity to the anomalies detected by the CT data, the NIR data and CT data need to be quantified. A qualitative correlation is present in Figure 14 as the intensity section of data shows an increase in spatter and geometrical representation of the desired part, as well as an increase in intensity. When laser power, and subsequently NIR signal intensity, increase there is an increase in density in the CT layer images.

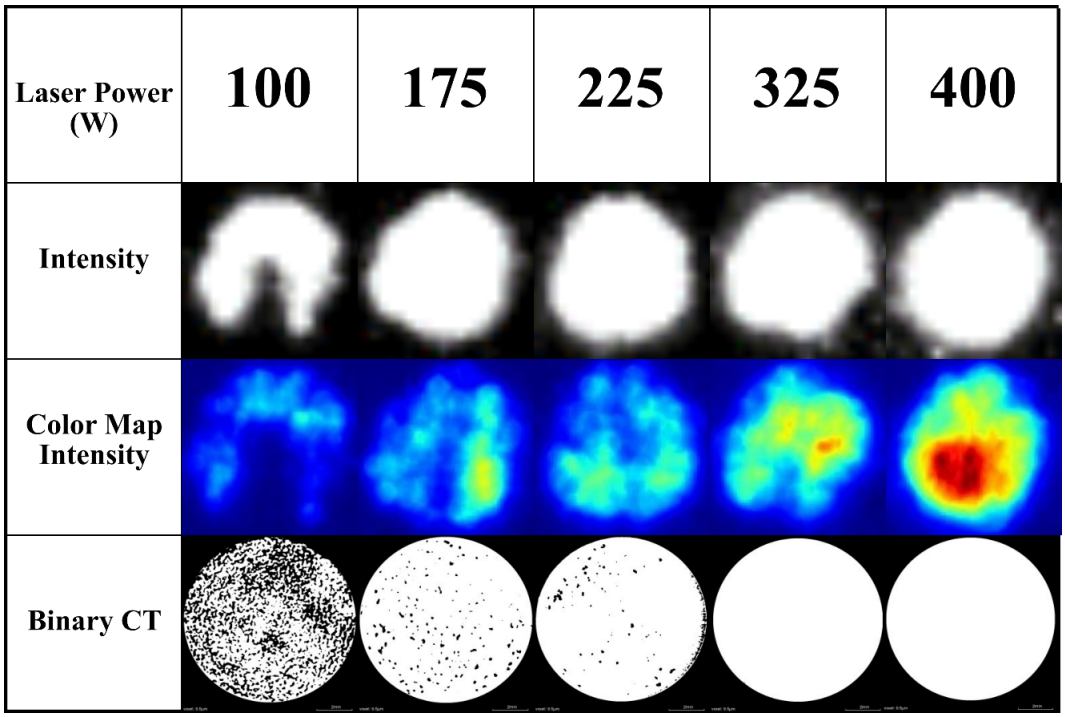

Figure 14: CT and NIR comparison.

To generate a quantitative correlation between the CT data and NIR data, a value was calculated as a representative indication of NIR intensity and CT density. The value calculated for NIR signals is cumulative NIR intensity which is the highest layer-wise cumulative pixel value from the layer analyzed in previous sections. The representative value for CT density was calculated by summing the number of non-empty voxels (these were identified as the pixels of the binary CT results that indicated 1 and not 0) for a designated region in all samples, as the samples all had different numbers of layers. The percentage of non-empty voxels was then calculated based on the sample considered to be fully dense (the highest number of non-empty voxels). The correlation between these two values can be seen in Figure 15. It can be seen that at NIR cumulative intensity values above 1500 yield final part densities above 90% while NIR cumulative intensity values below 1500 yield final part densities well below 60%, indicating severe porosity may exist.

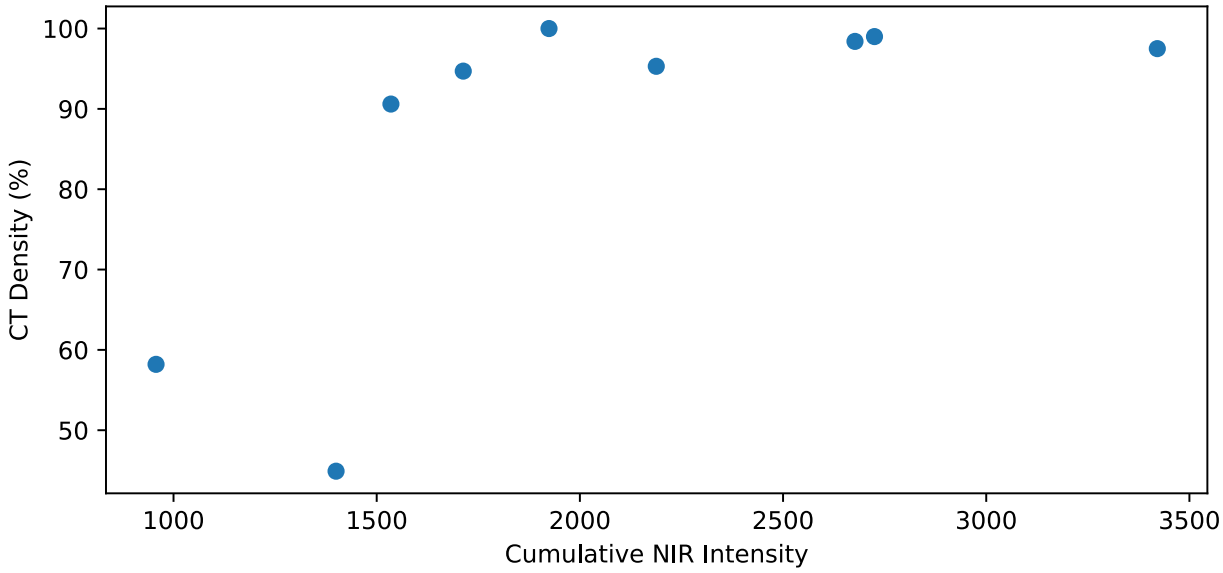

Figure 15: CT and NIR correlation

Conclusion

Through this research and others, it was noticed that IR cameras are expensive, slow, and yield low resolution. In many other published works, IR data has also been shown as still useful and valuable for additive manufacturing process monitoring. NIR data has been suggested to complement and possibly augment IR data [1]; however, this proved unfruitful for this research with our current system configuration.

The utility of NIR signal monitoring in L-PBF for process monitoring remains unresolved. We have shown that NIR cameras are capable of imaging interlayer temperatures or melt pool geometry, but not concurrently due to the different configurations needed with differing process conditions. The accumulated NIR intensity signals do correlate with global porosity trends, but future work is still required to resolve local porosity correlation.

Future work in this area of research aims at exploring geometrical defect detection, rather than global porosity detection. Other areas of exploration are the use of NIR as a powder bed temperature measurement device which would require the calibration of NIR signals to temperature and would allow for the ability to quantify thermal gradients with the merged IR and NIR data. More general areas for future work involve further refinement of the data visualization tools for easier identification of areas of interest, and finally implementing NIR signal collection into other additive manufacturing applications, such as wire-arc additive manufacturing.

References

[1] P. R. Gradl, A. C. Kimberlin, D. E. Gaddy, and R. D. Moody, "Method of Mapping Melt Pattern During Directed Energy Fabrication," 10688560, Jun. 23, 2020 Accessed: Jun. 22, 2022. [Online]. Available: https://patft.uspto.gov/netacgi/nph-Parser?Sect1=PTO1&Sect2=HITOFF&d=PALL&p=1&u=%2Fnetahtml%2FPTO%2Fsrchnum.htm&r=1&f=G&l=50&s1=10688560.PN.&OS=PN/10688560&RS=PN/10688560

[2] J. N. Zalameda *et al.*, "Calibrating IR cameras for in-situ temperature measurement during the electron beam melt processing of Inconel 718 and Ti-Al6-V4," presented at the Thermosense: Thermal Infrared Applications XXXVIII, 2016. doi: 10.1117/12.2229070.

[3] A. J. Dunbar and A. R. Nassar, “Assessment of optical emission analysis for in-process monitoring of powder bed fusion additive manufacturing,” *Virtual Phys. Prototyp.*, vol. 13, no. 1, pp. 14–19, 2017, doi: 10.1080/17452759.2017.1392683.
[4] M. Montazeri, A. R. Nassar, A. J. Dunbar, and P. Rao, “In-process monitoring of porosity in additive manufacturing using optical emission spectroscopy,” *IISE Trans.*, vol. 52, no. 5, pp. 500–515, 2019, doi: 10.1080/24725854.2019.1659525.